Application of an Improved Self-Starter to Geoacoustic Inversion

Robert J. Cederberg and Michael D. Collins

***Abstract*—The self-starter is improved using the operator of the split-step Padé solution. In addition to providing greater stability and being applicable closer to the source, the improved self-starter is an efficient forward model for geoacoustic inversion. It is necessary to solve only $O(10)$ tridiagonal systems of equations to obtain the acoustic field on a vertical array located $O(10)$ wavelengths from a source. This experimental configuration is effective for geoacoustic inverse problems involving unknown parameters deep in the ocean bottom. For problems involving depth-dependent acoustic parameters, the improved self-starter can be used to solve nonlinear inverse problems involving $O(10)$ unknown sediment parameters in less than a minute on the current generation of workstations.**

***Index Terms*—Coordinate rotation, geoacoustic inversion, parabolic wave equation, self-starter, simulated annealing, split-step Padé solution.**

I. Introduction

THE SELF-STARTER [1] is an efficient technique for generating initial conditions for parabolic wave equations [2]–[4]. In this paper, we improve the self-starter using the operator of the split-step Padé solution [5]. The improved self-starter provides greater stability, is applicable closer to the source, and may prove to be more efficient than separation-of-variables techniques for some range-independent problems. The improved self-starter is an efficient forward modeling tool for solving geoacoustic inverse problems that involve a source and a vertical array of receivers in the water column and unknown parameters in the ocean bottom. In Section II, we discuss outgoing wave equations, the self-starter, and the split-step Padé solution and derive the improved self-starter. In Section III, we discuss least-squares rational approximations and illustrate their accuracy in the sense of a function and as an operator for the self-starter. In Section IV, we show that the improved self-starter, simulated annealing [6]–[9], and a coordinate rotation technique [10] can be used to solve geoacoustic inverse problems involving $O(10)$ unknown parameters in less than a minute on the current generation of workstations. The self-starter is generalized to the near-field case in the Appendix.

II. The Improved Self-Starter

In this section, we derive the improved self-starter for the case of a line source in an ocean overlying a fluid sediment. We then apply a simple modification to obtain the solution for the point source case. The derivations are identical for the elastic and poroelastic [11] cases, with the exception that the scalar depth operators are replaced with matrices of operators [12]–[16]. We perform the derivation in Cartesian coordinates, with z being the depth below the ocean surface and the range x being the horizontal distance from a time–harmonic line source at $z = z_0$.

A vertical array of receivers is placed at $x = x_0$. Horizontal variations in the medium are assumed to be sufficiently gradual so that the region between the source and the array may be treated as range-independent. In this region, the complex pressure p satisfies

$$\frac{\partial^2 p}{\partial x^2} + Lp = 2i\delta(x)\delta(z - z_0) \tag{1}$$

$$L = \rho \frac{\partial}{\partial z} \frac{1}{\rho} \frac{\partial}{\partial z} + k^2 \tag{2}$$

where k is the wave number and ρ is the density. For $x > 0$, we factor the operator in (1) into a product of incoming and outgoing operators to obtain

$$\left(\frac{\partial}{\partial x} + iL^{1/2}\right)\left(\frac{\partial}{\partial x} - iL^{1/2}\right)p = 0. \tag{3}$$

Assuming that outgoing energy dominates incoming energy, we obtain the outgoing wave equation

$$\frac{\partial p}{\partial x} = iL^{1/2}p. \tag{4}$$

Parabolic equation solutions are obtained by approximating the operator square root in (4) to obtain an equation that can be solved using standard numerical techniques to discretize in range and depth [17], with grid spacings that are smaller than a wavelength. Improved efficiency may be achieved by first solving (4) formally to obtain

$$p(x + \Delta x, z) = \exp\left(i\Delta x L^{1/2}\right)p(x, z) \tag{5}$$

where Δx is the range step. The split-step Padé solution is obtained by approximating the exponential of the operator square root in (5) and then applying numerical techniques to discretize in depth. The advantage of this approach is that the higher order truncation error in the range numerics permits range steps of many wavelengths rather than a fraction of a wavelength [5].

Prior to solving (4) and (5), it is necessary to specify an initial condition. The self-starter is an efficient approach for obtaining an initial condition. Integrating (1) over an

Manuscript received March 11, 1996; revised July 30, 1996.

The authors are with the Naval Research Laboratory, Washington, DC 20375 USA.

Publisher Item Identifier S 0364-9059(97)00868-6.

arbitrarily small range interval about the origin and applying the symmetry of the source condition, we obtain

$$\lim_{x \to 0^+} \frac{\partial p}{\partial x} = i\delta(z - z_0). \tag{6}$$

Applying (4) to replace the range operator in (6), we obtain

$$L^{1/2} p = \delta(z - z_0). \tag{7}$$

This initial condition cannot be evaluated numerically because it is singular at $z = z_0$. An approach for obtaining an initial condition away from $x = 0$ is described in [1]. The singularity is not of concern for the improved self-starter because the field is desired at $x = x_0$.

Combining (5) and (7) for the case $x = 0$ and $\Delta x = x_0$, we obtain

$$p(x_0, z) = \exp(ix_0 L^{1/2}) L^{-1/2} \delta(z - z_0). \tag{8}$$

In the far field, the line source and point source solutions differ in the powers of k_j that appear in the normal mode solution [18], [19], where the jth eigenvalue k_j^2 is defined in the appendix. The factor $L^{-1/2}$ in (8) provides the factor of k_j^{-1} that appears in the line source solution. The factor $L^{-1/4}$ is required to obtain the factor of $k_j^{-1/2}$ that appears in the point source solution. The solution for a point source is therefore proportional to

$$p(r_0, z) = r_0^{-1/2} \exp(ir_0 L^{1/2}) L^{-1/4} \delta(z - z_0) \tag{9}$$

where r_0 is the range of the array and the factor of $r_0^{-1/2}$ accounts for cylindrical spreading. The far-field expression in (9) breaks down when r_0 is comparable to a representative wavelength. In the appendix, we discuss an expression that is valid in the near field.

We let k_0 be a representative wave number and define the operator

$$X = k_0^{-2}(L - k_0^2) \tag{10}$$

so that (9) becomes

$$\begin{aligned} p(r_0, z) =& (k_0 r_0)^{-1/2} \exp(ik_0 r_0 (1 + X)^{1/2}) \\ & \times (1 + X)^{-1/4} \delta(z - z_0). \end{aligned} \tag{11}$$

Although the left side of (11) (the final result) is not singular, it is necessary to use caution when solving (11) to avoid encountering intermediate results that are singular. We therefore rearrange (11) and obtain

$$\begin{aligned} p(r_0, z) =& (k_0 r_0)^{-1/2} (1 + X)^{7/4} \\ & \times \exp(ik_0 r_0 (1 + X)^{1/2}) \sigma(z) \end{aligned} \tag{12}$$

$$(1 + X)^2 \sigma(z) = \delta(z - z_0) \tag{13}$$

where $\sigma(z)$ is twice differentiable at $z = z_0$. We solve (12) using a rational approximation in X. Rational approximations have been used to solve (4), (5), and (7) for the acoustic [1], [5], [17], [20]–[23], elastic [12]–[15], and poroelastic [16] cases. In principle, efficiency may be improved slightly by using the factor $1 + X$ in (13) and the factor $(1 + X)^{3/4}$ in (12) so that $\sigma(z)$ is merely continuous at $z = z_0$. We do not recommend this approach because the cusp in $\sigma(z)$ at $z = z_0$ can cause a degradation in accuracy and stability. The solution of (13) may be obtained using standard numerical approaches as discussed in [1].

We replace the operator in (12) with the rational approximation

$$\begin{aligned} (1 + X)^{7/4} & \exp(ik_0 r_0 (1 + X)^{1/2}) \\ & \cong \exp(ik_0 r_0) \prod_{j=1}^{n} \frac{1 + \alpha_{j,n} X}{1 + \beta_{j,n} X} \end{aligned} \tag{14}$$

where n and the coefficients $\alpha_{j,n}$ and $\beta_{j,n}$ (which depend on $k_0 r_0$) are chosen to provide accuracy and stability. We discuss constraints for defining the coefficients and an approach for obtaining them in Section III. Substituting (14) into (12), we obtain

$$p(r_0, z) = \frac{\exp(ik_0 r_0)}{(k_0 r_0)^{1/2}} \prod_{j=1}^{n} \frac{1 + \alpha_{j,n} X}{1 + \beta_{j,n} X} \sigma(z). \tag{15}$$

Expanding the rational function by partial fractions, we obtain

$$p(r_0, z) = \frac{\exp(ik_0 r_0)}{(k_0 r_0)^{1/2}} \left(1 + \sum_{j=1}^{n} \frac{\gamma_{j,n} X}{1 + \beta_{j,n} X} \right) \sigma(z). \tag{16}$$

Since the terms on the right side of (16) may be evaluated in parallel, the improved self-starter is well suited to computers with n processors. Since the sum form of the rational function is more sensitive to round-off errors, the product form should be used for single-processor applications. Although rational approximations have proved to be robust for PE applications, it is necessary to use care to ensure that the evanescent spectrum is annihilated properly, especially for problems involving elastic or poroelastic layers [14]–[16].

The improved self-starter has several advantages over the original self-starter. The original self-starter is described in terms of a relatively complicated sequence of steps (apply an operator, march the field in range using the square root of an operator, and finally apply another operator); the improved self-starter is described in terms of a single operator in (11). The improved self-starter provides greater efficiency; the original self-starter involves marching the field in range with a finite-difference PE algorithm, which requires small range steps due to limited accuracy in $k_0 \Delta r$; the improved self-starter is based on the split-step Padé solution, which provides higher order accuracy in $k_0 r_0$. The efficiency gain is marginal for problems involving long-range propagation because the effort required to march the field out in range dominates the effort required to compute the self-starter; the efficiency gain is significant for the geoacoustic inverse problem because no marching is involved. The original self-starter was implemented using rational approximations that provide accurate PE solutions at long ranges; with the improved rational approximations described in Section III, the self-starter is accurate at the relatively short ranges of interest for the geoacoustic inverse problem.

The numerical implementation of the improved self-starter involves the solution of $n + 2$ tridiagonal systems of equations. When the array is located $O(10)$ wavelengths from the

source, the self-starter provides accurate solutions for $n = O(10)$ and may prove to be more efficient than separation-of-variables techniques. Normal mode solutions typically require the solution of $O(10^3)$ or more tridiagonal systems. According to large-range asymptotic estimates that are implicit in [24], wave-number integration solutions [25], [26] require the solution of $O(10)$ tridiagonal systems for ranges of $O(10)$ wavelengths. For small ranges, however, the required sampling may depend on the complexity of the wave number spectrum rather than the rate of oscillation of the Bessel function (which is the basis for the large-range asymptotics). Although it is possible to reduce sampling by displacing the integration contour off the real axis [24], $O(10)$ samples are not sufficient in general even when special integration techniques [27] are applied.

Although the improved self-starter may be more efficient when the field is only desired at a particular range, the separation-of-variables techniques provide the field at all ranges once the tridiagonal systems have been solved. Another advantage of separation-of-variables techniques is that they may be implemented using piecewise analytic functions for problems involving homogeneous layers (it might be possible to apply this approach to the self-starter). When the depth dependence is relatively simple, these techniques can be more efficient than the self-starter as it is presently implemented. For the application to geoacoustic inversion in Section IV, however, the depth dependence is often relatively complex.

III. Implementation and Testing

In this section, we discuss an efficient approach for deriving rational approximations and illustrate their accuracy for application to the improved self-starter. We define

$$f(X) = (1+X)^{7/4} \exp\left[ik_0 r_0(-1+(1+X)^{1/2})\right] \quad (17)$$

$$g(X) = \left(1+\sum_{j=1}^{n} a_{j,n} X^j\right)\left(1+\sum_{j=1}^{n} b_{j,n} X^j\right)^{-1} \quad (18)$$

where the coefficients $a_{j,n}$ and $b_{j,n}$ are to be determined to that $g(X)$ approximates $f(X)$. There are various choices for constraints to define the coefficients. We require that the coefficients provide the best least squares fit to the equations:

$$1+\sum_{j=1}^{n} a_{j,n} X_i^j = f(X_i)\left(1+\sum_{j=1}^{n} b_{j,n} X_i^j\right) \quad (19)$$

where the X_i are the matching points.

We select most of the X_i from an interval near $X = 0$ (the accuracy constraints) and the rest of the X_i from $X < -1$ so that evanescent modes decay with range (the stability constraints). We select a sufficient number of points in the accuracy interval so that the error is distributed relatively uniformly. The appropriate constraints are problem dependent. For example, accuracy may be required over a wider interval when r_0 is relatively small because energy that is not trapped in the water column may be important. The least-squares problem for the coefficients in (19) is linear. Once the coefficients are determined, an approximation of the form appearing in (14) may be obtained by finding the roots of the polynomials in (18). This approach is more efficient than directly obtaining a rational approximation in the form of (14) using Newton's method [28].

We have investigated the effectiveness of other types of constraints for the rational approximations. An important class of approximations for parabolic equation applications is obtained by requiring that several derivatives of $g(X)$ are correct at $X = 0$ and including a small number of stability constraints. These approximations are ideal for the split-step Padé approximation because the propagating spectrum must be handled very accurately for long-range propagation. The least-squares approximations are ideal when the field is desired at short ranges because accuracy is required at a moderate level over a wide part of the propagating spectrum and the evanescent spectrum must be annihilated rapidly.

We test the accuracy of the rational approximation and the self-starter with example A, which involves a 35-Hz source at $z = 290$ m in a 300-m-deep water column, with $n = 12$ and $r_0 = 500$ m. The sound speed is 1500 m/s in the homogeneous water column. In the homogeneous sediment, the sound speed is 1700 m/s, the density is 1.5 g/cm^3, and the attenuation is 0.5 dB/λ. We were able to obtain accurate solutions with the self-starter by placing thirty of the X_i in $-0.7 \le X \le 0$ (the accuracy constraints) and ten of the X_i in $-2 \le X \le -1.1$ (the stability constraints) and taking $k_0 = \omega c_0^{-1}$, where $c_0 = 1500$ m/s. The functions $f(X)$ and $g(X)$ are compared in Fig. 1. The rational approximation is accurate in $-0.7 \le X \le 0$ (so that propagating modes are handled accurately) and maps the region $X < -1$ to small values (so that evanescent modes are annihilated). Since the rational approximation cannot handle the branch point $X = -1$, it breaks down in $-1 \le X \le -0.7$. The self-starter solution appearing in Fig. 2 is in agreement with a reference solution that was generated using a normal mode model [29].

IV. Application to Geoacoustic Inversion

Forward models are important tools for solving inverse problems. Efficiency is a key issue for nonlinear inverse problems, which often require a large number of forward solutions. In this section, we show that the improved self-starter is an efficient tool for solving geoacoustic inverse problems involving unknown parameters in the ocean bottom. There has recently been an interest in applying nonlinear optimization techniques to this problem [30]–[33]. Good agreement with data has been achieved [30] using simulated annealing. The performance of the parameter search can be improved by rotating coordinates to optimally align the parameter axes with the most prominent valleys in the parameter landscape [10]. Both horizontal and vertical arrays have advantages for the geoacoustic inverse problem. Synthetic aperture horizontal arrays [34]–[35] require a minimal amount of hardware and are capable of resolving range dependence in the ocean-bottom parameters. A vertical array placed relatively close to the source can probe deeply into the ocean bottom.

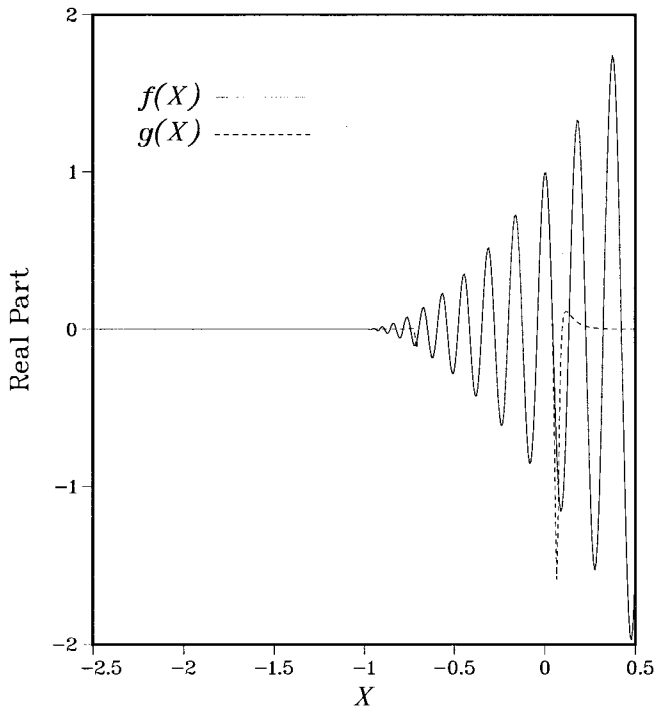

(a)

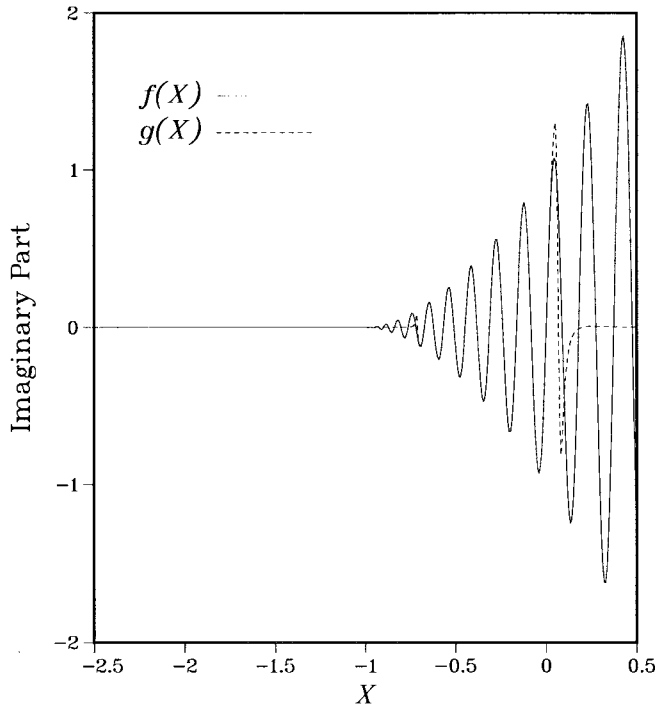

(b)

Fig. 1. The accuracy of the rational approximation for example A. Comparison of the functions defined in (17) and (18) for $r_0 = 500$ m. The real and imaginary parts of $g(X)$ are nearly identical to the real and imaginary parts of $f(X)$ away from a region near the branch point $X = -1$.

We consider the case of a vertical array of receivers located in the water column at $r = r_0$. The self-starter is an efficient forward model for this problem when $r_0 = O(10)$ wavelengths. The jth entry of the parameter vector $\mathbf{x}$ that describes the ocean bottom is x_j. The jth entry of the complex

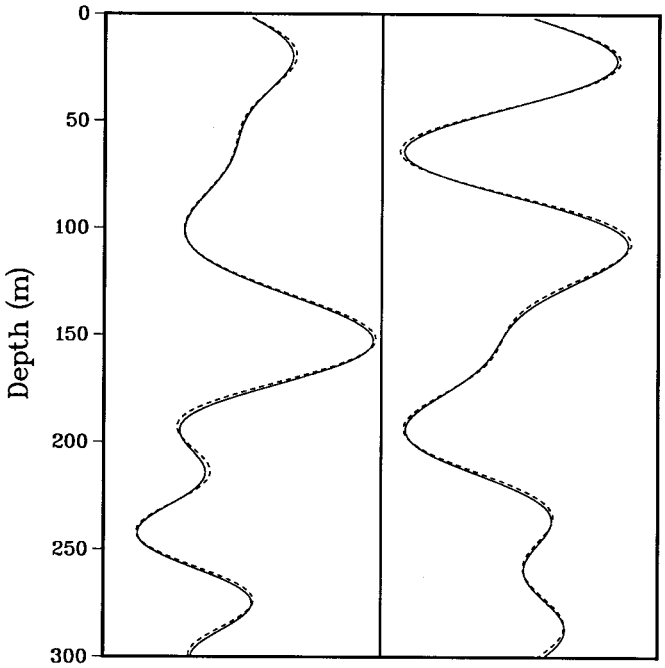

Fig. 2. The accuracy of the self-starter for example A. Comparison of the complex pressures at $r = 500$ m generated with the self-starter (solid curves) and a normal mode model (dashed curves). Both the real (left panel) and imaginary (right panel) parts of the complex pressure are in agreement.

pressure vector $\mathbf{p}(\mathbf{x})$ is $p(r_0, z_j)$, where z_j is the depth of the jth receiver in the array. We use the cost function

$$E(\mathbf{x}) = \sqrt{1 - |\hat{\mathbf{p}}^*(\mathbf{x}) \cdot \hat{\mathbf{p}}(\mathbf{x}_0)|^2} \tag{20}$$

where $\hat{\mathbf{p}}$ is the normalized complex pressure vector, the superscript asterisk indicates complex conjugation, $\mathbf{x}_0$ is the desired geoacoustic data, and $\hat{\mathbf{p}}(\mathbf{x}_0)$ is the measured acoustic data.

We solve the optimization problem using the simulated annealing algorithm discussed in [30] and the coordinate rotation discussed in [10]. The purpose of the coordinate rotation is to improve the efficiency of the parameter search for problems involving long valleys (i.e., coupling between parameters). The parameter space is

$$\Omega = \{\mathbf{x} \mid A_j < x_j < B_j\} \tag{21}$$

where A_j and B_j are the bounds on the jth parameter. The basis vectors $\{\mathbf{v}_j\}$ for the optimal rotation are the eigenvectors of the covariance matrix

$$K = \int_\Omega \nabla E (\nabla E)^t \, d\Omega. \tag{22}$$

The integral in (22) may be evaluated efficiently with the Monte Carlo method [36], [37], even when the dimension of $\mathbf{x}$ is large. Since the integral

$$I_j = \int_\Omega (\mathbf{v}_j \cdot \nabla E)^2 \, d\Omega \tag{23}$$

is stationary with respect to rotations of $\mathbf{v}_j$, the rotated coordinate axes are optimally aligned with the most prominent

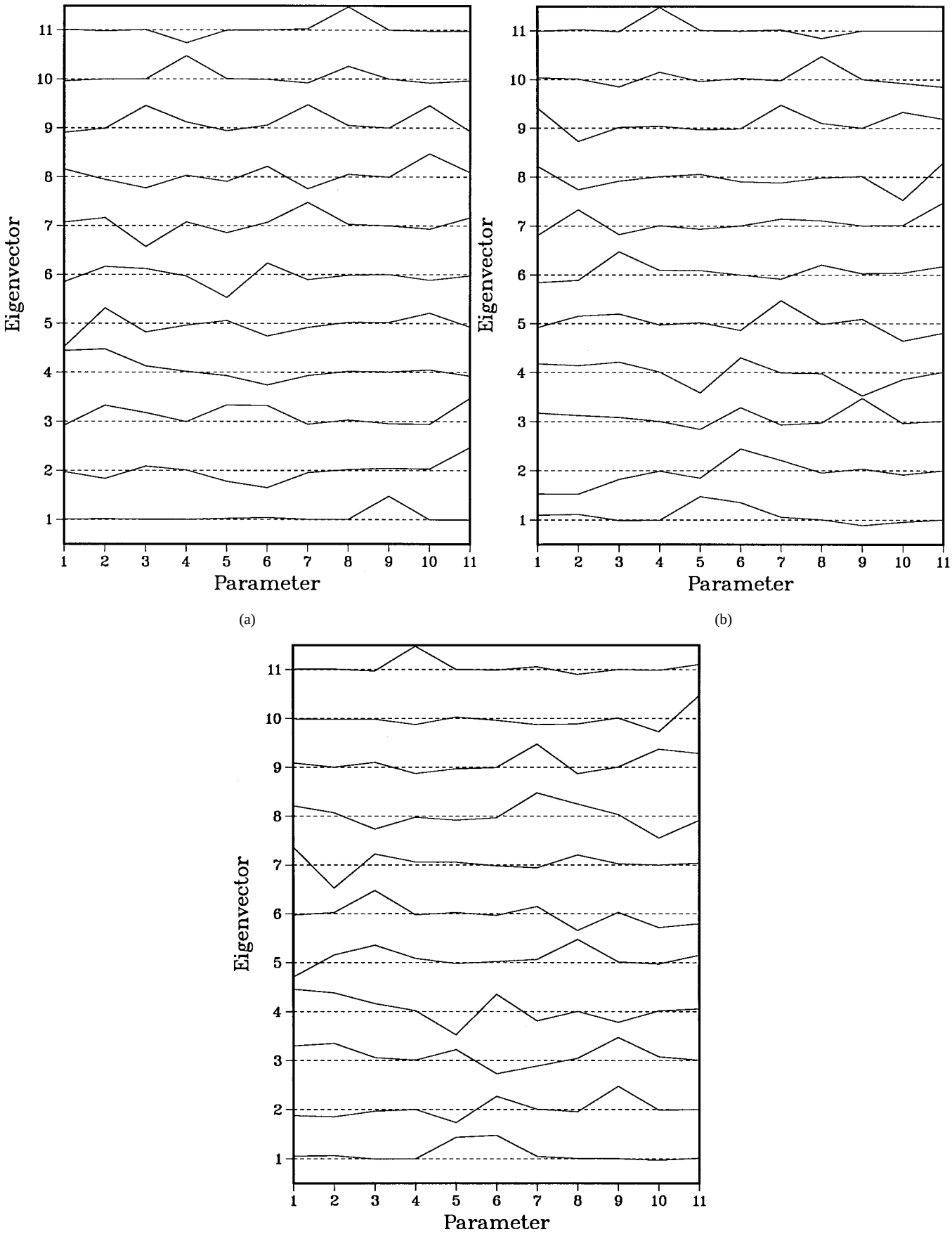

(a)

(b)

(c)

Fig. 3. The coordinate rotation for example B. The eigenvectors of the covariance matrix of the cost function for the cases (a) $r_0 = 200$ m, (b) $r_0 = 500$ m, and (c) $r_0 = 1$ km. The order of the eigenvectors corresponds to decreasing eigenvalue so that the lower eigenvectors represent the best resolved underlying parameters.

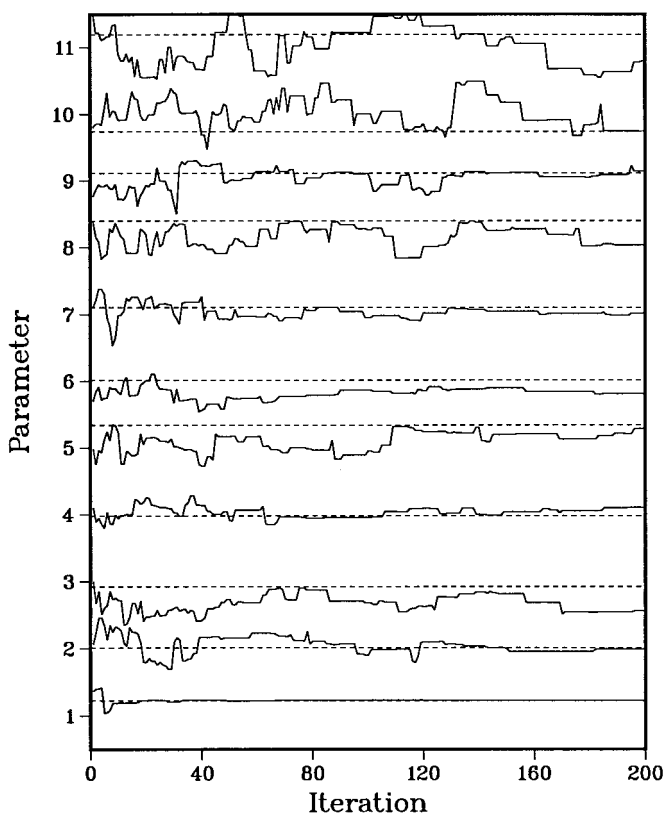

(a)

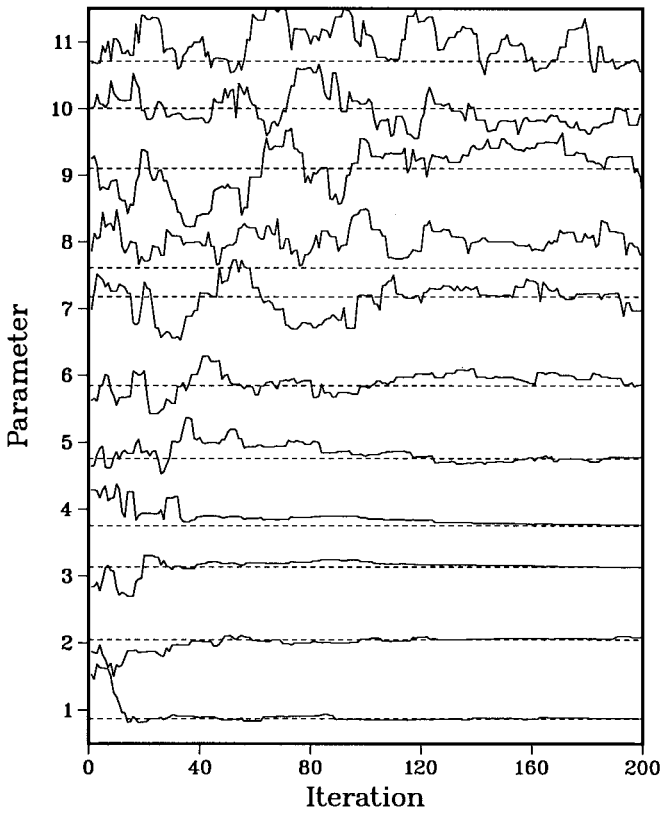

(b)

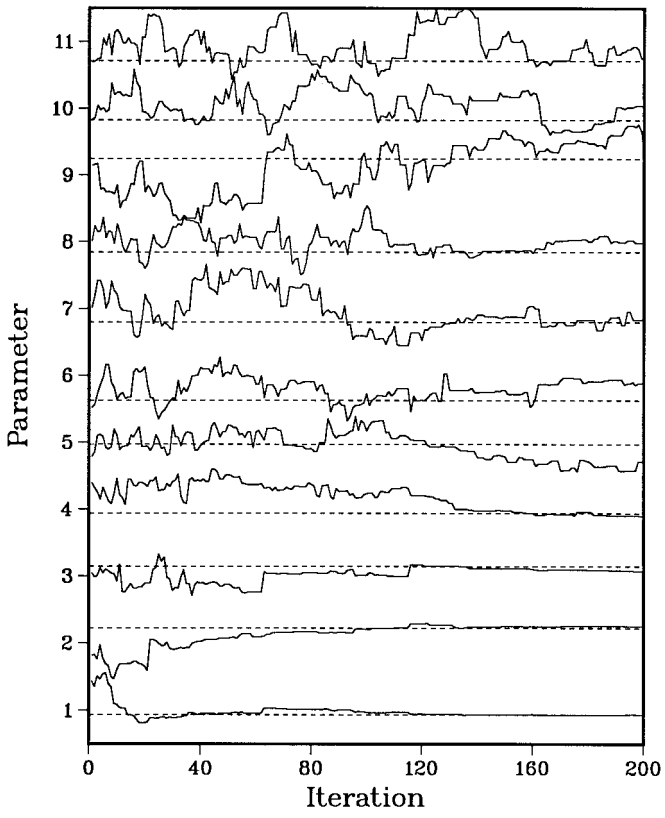

(c)

Fig. 4. The searches for the rotated parameters for example B for the cases (a) $r_0 = 200$ m, (b) $r_0 = 500$ m, and (c) $r_0 = 1$ km. The dashed lines indicate the true values of the rotated parameters.

TABLE I
PARAMETER VALUES AND BOUNDS FOR EXAMPLE B

j	x_j	A_j	B_j	units
1	1625	1550	1750	m/s
2	1670	1550	1750	m/s
3	1.2	1.1	1.5	g / cm^3
4	0.1	0.05	0.3	dB / λ
5	1700	1600	1850	m/s
6	1730	1600	1850	m/s
7	1.3	1.1	1.5	g / cm^3
8	0.2	0.05	0.3	dB / λ
9	1800	1650	1850	m/s
10	1.5	1.1	1.5	g / cm^3
11	0.3	0.1	0.5	dB / λ

valleys of the parameter landscape. The eigenvectors that correspond to the largest eigenvalues indicate the most resolvable underlying parameters.

Example B involves a 35-Hz source at $z = 290$ m in a 300-m-deep water column. The ocean bottom consists of two sediment layers overlying a homogeneous half space basement. In each sediment layer, the sound speed is linear and the density and attenuation are constant. The parameters in the 15-m-thick top sediment layer are the sound speeds x_1 and x_2 at the top and bottom of the layer, the density x_3, and the attenuation x_4. The parameters in the 50-m-thick lower sediment layer are the sound speeds x_5 and x_6 at the top and bottom of the layer, the density x_7, and the attenuation x_8. The parameters in the basement are the sound speed x_9, the density x_{10}, and the attenuation x_{11}. The values and ranges of the parameters are given in Table I. We take $n = 12$ and $z_j = (-10+20j)$ m for $1 \le j \le 15$ and consider the cases $r_0 = 200$ m, $r_0 = 500$ m, and $r_0 = 1$ km. We use the stability constraints of example A for each case and the accuracy constraints of example A for the case $r_0 = 500$ m. We place the accuracy constraints on $-0.9 \le X \le 0$ for $r_0 = 200$ m and on $-0.5 \le X \le 0$ for $r_0 = 1$ km.

The eigenvectors of the covariance matrix appear in Fig. 3 for each of the array locations. The sound speeds are the best resolved parameters. Since the array probes deeper into the sediment when it is closer to the source, x_9 is the best resolved parameter for the case $r_0 = 200$ m. There is strong coupling between parameters for each of the array locations. For example, the sound-speed gradient of the lower sediment layer appears in v_2, v_3, and v_4 for the cases $r_0 = 500$ m and $r_0 = 1$ km so that this parameter is intertwined with several other parameters. Simulated annealing results for example B appear in Fig. 4 for each of the array locations. Each of the parameter searches involved 200 iterations and 2200 sets of replica fields and required 37 s of computation time on a Silicon Graphics computer with a MIPS R8000 processor. Two parameters are resolved reliably for the case $r_0 = 200$ m. Five parameters are resolved reliably for $r_0 = 500$ m, which is the most effective of the three array locations. Four parameters are resolved reliably for the case $r_0 = 1$ km.

V. CONCLUSION

The improved self-starter is based on an operator that is a product of the operators of the original self-starter and the split-step Padé solution. Rational approximations designed for the improved self-starter provide accurate and stable solutions of the acoustic wave equation. The improvements also apply to problems involving elastic and poroelastic layers. With the self-starter as the forward model, it is possible to solve geoacoustic inverse problems involving a source and vertical array of receivers in the water column in less than a minute on the current generation of workstations.

APPENDIX
THE NEAR-FIELD PROBLEM

The standard approach for deriving parabolic equation techniques in cylindrical geometry is to begin with the far-field equation. In this appendix, we generalize the self-starter to short ranges. In cylindrical geometry, the normal mode solution at $r = r_0$ is proportional to

$$p(r_0, z) = \sum_j \phi_j(z_0)\phi_j(z)H_0^{(1)}(k_j r_0) \tag{24}$$

where the jth eigenfunction ϕ_j and eigenvalue k_j^2 satisfy

$$k_0^2(1+X)\phi_j = k_j^2\phi_j. \tag{25}$$

The self-starter requires a near-field correction when the far-field asymptotic form of the Hankel function breaks down for any of the significant terms in (24). As (25) indicates, the operator $k_0(1+X)^{1/2}$ reduces to scalar multiplication in mode space. From the following representation of the delta function

$$\delta(z - z_0) = \sum_j \phi_j(z_0)\phi_j(z) \tag{26}$$

we therefore obtain

$$p(r_0, z) = h(X)\delta(z - z_0) \tag{27}$$

$$h(X) = H_0^{(1)}(k_0 r_0(1+X)^{1/2}). \tag{28}$$

Near-field problems may be solved using (27), which reduces to (11) (modulo a constant factor) in the limit $k_0 r_0 \gg 1$. The implementation involves a rational approximation for $(1+X)^2 h(X)$ and the intermediate solution $\sigma(z)$ defined in (13).

REFERENCES

[1] M. D. Collins, "A self-starter for the parabolic equation method," *J. Acoust. Soc. Amer.*, vol. 92, pp. 2069–2074, 1992.
[2] M. A. Leontovich and V. A. Fock, "Solution of the problem of propagation of electromagnetic waves along the earth's surface by the method of parabolic equation," *J. Exp. Theor. Phys.*, vol. 16, pp. 557–573, 1946.
[3] V. A. Fock, *Electromagnetic Diffraction and Propagation Problems.* New York: Pergamon, 1965, pp. 213–234.

[4] F. D. Tappert, "The parabolic approximation method," in *Wave Propagation and Underwater Acoustics* (Lecture Notes in Physics, vol. 70), J. B. Keller and J. S. Papadakis, Eds. New York: Springer, 1977, pp. 224–280.
[5] M. D. Collins, "A split-step Padé solution for the parabolic equation method," *J. Acoust. Soc. Amer.*, vol. 93, pp. 1736–1742, 1993.
[6] N. Metropolis, A. W. Rosenbluth, M. N. Rosenbluth, A. H. Teller, and E. Teller, "Equations of state calculations by fast computing machines," *J. Chem. Phys.*, vol. 21, pp. 1087–1091, 1953.
[7] S. Kirkpatrick C. D. Gellatt, and M. P. Vecchi, "Optimization by simulated annealing," *Science*, vol. 220, pp. 671–680, 1983.
[8] H. Szu and R. Hartley, "Fast simulated annealing," *Phys. Lett.*, vol. 122, pp. 157–162, 1987.
[9] A. Basu and L. N. Frazer, "Rapid determination of critical temperature in simulated annealing inversion," *Science*, vol. 249, pp. 1409–1412, 1990.
[10] M. D. Collins and L. Fishman, "Efficient navigation of parameter landscapes," *J. Acoust. Soc. Amer.*, vol. 98, pp. 1637–1644, 1995.
[11] M. A. Biot, "Theory of propagation of elastic waves in a fluid-saturated porous solid," *J. Acoust. Soc. Amer.*, vol. 28, pp. 168–191, 1956.
[12] R. R. Greene, "A high-angle one-way wave equation for seismic wave propagation along rough and sloping interfaces," *J. Acoust. Soc. Amer.*, vol. 77, pp. 1991–1998, 1985.
[13] M. D. Collins, "A higher-order parabolic equation for wave propagation in an ocean overlying an elastic bottom," *J. Acoust. Soc. Amer.*, vol. 86, pp. 1459–1464, 1989.
[14] B. T. R. Wetton and G. H. Brooke, "One-way wave equations for seismoacoustic propagation in elastic waveguides," *J. Acoust. Soc. Amer.*, vol. 87, pp. 624–632, 1990.
[15] M. D. Collins, "Higher-order Padé approximations for accurate and stable elastic parabolic equations with application to interface wave propagation," *J. Acoust. Soc. Amer.*, vol. 89, pp. 1050–1057, 1991.
[16] M. D. Collins, W. A. Kuperman, and W. L. Siegmann, "A parabolic equation for poro-elastic media," *J. Acoust. Soc. Amer.*, vol. 98, pp. 1645–1656, 1995.
[17] M. D. Collins, "Applications and time-domain solution of higher-order parabolic equations in underwater acoustics," *J. Acoust. Soc. Amer.*, vol. 86, pp. 1097–1102, 1989.
[18] R. B. Evans, "A coupled mode solution for acoustic propagation in a waveguide with stepwise depth variations of a penetrable bottom," *J. Acoust. Soc. Amer.*, vol. 74, pp. 188–195, 1983.
[19] M. B. Porter and E. L. Reiss, "A numerical method for ocean acoustic modes," *J. Acoust. Soc. Amer.*, vol. 76, pp. 244–252, 1984.
[20] J. F. Claerbout, *Fundamentals of Geophysical Data Processing.* New York: McGraw-Hill, 1976, pp. 206–207.
[21] G. Botseas, D. Lee, and K. E. Gilbert, "IFD: Wide-angle capability," NUSC, New London, CT, NUSC Tech Rep. 6905, 1983.
[22] R. R. Greene, "The rational approximation to the acoustic wave equation with bottom interaction," *J. Acoust. Soc. Amer.*, vol. 76, pp. 1764–1773, 1984.
[23] A. Bamberger, B. Engquist, L. Halpern, and P. Joly, "Higher order paraxial wave equation approximations in heterogeneous media," *SIAM J. Appl. Math.*, vol. 48, pp. 129–154, 1988.
[24] F. B. Jensen, W. A. Kuperman, M. B. Porter, and H. Schmidt, *Computational Ocean Acoustics.* New York: American Inst. Phys., 1994, pp. 231–243.
[25] F. R. DiNapoli, "Theoretical and numerical Green's function solution in a plane multilayered medium," *J. Acoust. Soc. Amer.*, vol. 67, pp. 92–105, 1980.
[26] H. Schmidt and F. B. Jensen, "A full wave solution for propagation in multilayered viscoelastic media with application to Gaussian beam reflection at fluid-solid interfaces," *J. Acoust. Soc. Amer.*, vol. 77, pp. 813–825, 1985.
[27] S. Ivansson and I. Karasalo, "A high-order adaptive integration method for wave propagation in range-independent fluid-solid media," *J. Acoust. Soc. Amer.*, vol. 92, pp. 1569–1577, 1992.
[28] M. D. Collins, "Generalization of the split-step Padé solution," *J. Acoust. Soc. Amer.*, vol. 96, pp. 382–385, 1994.
[29] M. Porter, "The KRAKEN normal mode program," SACLANT Undersea Research Centre, La Spezia, Italy, SACLANTCEN SM-245, 1991.
[30] M. D. Collins, W. A. Kuperman, and H. Schmidt, "Nonlinear inversion for ocean-bottom properties," *J. Acoust. Soc. Amer.*, vol. 92, pp. 2770–2783, 1992.
[31] C. E. Lindsay and N. R. Chapman, "Matched field inversion for geoacoustic model parameters using adaptive simulated annealing," *IEEE J. Oceanic Eng.*, vol. 18, pp. 224–238, 1993.
[32] S. E. Dosso, M. L. Yeremy, J. M. Ozard, and N. R. Chapman, "Estimation of ocean bottom properties by matched-field inversion of acoustic field data," *IEEE J. Oceanic Eng.*, vol. 18, pp. 232–239, 1993.
[33] P. Gerstoft, "Inversion of acoustic data using a combination of genetic algorithms and the Gauss-Newton approach," *J. Acoust. Soc. Amer.*, vol. 97, pp. 2181–2190, 1995.
[34] J. F. Lynch, S. D. Rajan, and G. V. Frisk, "A comparison of broadband and narrow-band modal inversions for bottom properties at a site near Corpus Christi, Texas," *J. Acoust. Soc. Amer.*, vol. 89, pp. 648–665, 1991.
[35] R. J. Cederberg, W. L. Siegmann, and W. M. Carey, "Influence of geoacoustic modeling on predictability of low-frequency propagation in range-dependent, shallow-water environments," *J. Acoust. Soc. Amer.*, vol. 97, pp. 2754–2766, 1995.
[36] P. J. Davis and P. Rabinowitz, *Methods of Numerical Integration.* New York: Academic, 1984, pp. 384–393.
[37] M. H. Kalos and P. A. Whitlock, *Monte Carlo Methods.* New York: Wiley, 1986, pp. 89–116.

Robert J. Cederberg was born in Fargo, ND, on February 20, 1964. He received the B.S. degree in computer science and mathematics and the M.S. degree in mathematics from North Dakota State University, Fargo, in 1986 and 1988, respectively, and the Ph.D. degree in mathematics from Rensselaer Polytechnic Institute (RPI), Troy, NY, in 1993.

He was a Post-Doctoral Research Associate in the Department of Mathematical Sciences at RPI from January 1994 to August 1994. Since then, he has held a National Research Council Research Associateship in the Acoustics Division of the Naval Research Laboratory, Washington, DC. His research has focused on shallow-water acoustic propagation modeling.

Dr. Cederberg is a member of the Acoustical Society of America and the Society of Industrial and Applied Mathematics.

Michael D. Collins was born in Greenville, PA, in 1958. He received the B.S. degree in mathematics from the Massachusetts Institute of Technology, Cambridge, in 1982, the M.S. degree in mathematics from Stanford University, Stanford, CA, in 1986, and the Ph.D. degree in applied mathematics from Northwestern University, Evanston, IL, in 1988.

Since 1989, he has worked for the Naval Research Laboratory. During 1985–1989, he worked at the Naval Ocean Research and Development Activity, Stennis Space Center, MS (which is now NRL-SSC) as both a civilian employee and as an on-site representative of SYNTEK Engineering and Computer Systems, Inc., Rockville, MD.

Dr. Collins is a member of the Acoustical Society of America, the Society for Industrial and Applied Mathematics, and the American Geophysical Union.